Nanoscale Advances

ROYAL SOCIETY OF CHEMISTRY

PAPER

View Article Online
View Journal | View Issue

Check for updates

Cite this: *Nanoscale Adv.*, 2023, **5**, 2517

A novel long-acting antimicrobial nanomicelle spray†

Mousa El-Sayed,[a] Saif El-Din Al-Mofty,[a] Noha Khalil Mahdy,[a] Wessam Awad Sarhan*[a] and Hassan Mohamed El-Said Azzazy *[ab]

Contaminated surfaces play a major role in disease transmission to humans. The vast majority of commercial disinfectants provide short-term protection of surfaces against microbial contamination. The Covid-19 pandemic has attracted attention to the importance of long-term disinfectants as they would reduce the need for staff and save time. In this study, nanoemulsions and nanomicelles containing a combination of benzalkonium chloride (BKC; a potent disinfectant and a surfactant) and benzoyl peroxide (BPO; a stable form of peroxide that is activated upon contact with lipid/membranous material) were formulated. The prepared nanoemulsion and nanomicelle formulas were of small sizes <80 nm and high positive charge >45 mV. They showed enhanced stability and prolonged antimicrobial efficacy. The antibacterial potency was evaluated in terms of long-term disinfection on surfaces as verified by repeated bacterial inoculums. Additionally, the efficacy of killing bacteria upon contact was also investigated. A nanomicelle formula (NM-3) consisting of 0.8% BPO in acetone and 2% BKC plus 1% TX-100 in distilled water (1 : 5 volume ratio) demonstrated overall surface protection over a period of 7 weeks upon a single spray application. Furthermore, its antiviral activity was tested by the embryo chick development assay. The prepared NM-3 nanoformula spray showed strong antibacterial activities against *Pseudomonas aeruginosa*, *Escherichia coli*, and *Staphylococcus aureus* as well as antiviral activities against infectious bronchitis virus due to the dual effects of BKC and BPO. The prepared NM-3 spray shows great potential as an effective solution for prolonged surface protection against multiple pathogens.

Received 26th December 2022
Accepted 20th March 2023

DOI: 10.1039/d2na00950a

rsc.li/nanoscale-advances

Open Access Article. Published on 21 March 2023. Downloaded on 2/11/2026 2:45:44 PM.
This article is licensed under a Creative Commons Attribution-NonCommercial 3.0 Unported Licence.

Introduction

Any individual risks developing an infection upon touching contaminated surfaces. This risk becomes more likely in health care facilities. This represents a major public health risk and a huge economic burden. Subsequently, the utilization of disinfectants has surged for those available commercially such as 70% ethanol, 0.1% sodium hypochlorite, or 0.5% hydrogen peroxide. Nevertheless, these are considered temporary solutions with reported side effects.[1,2] Thus, this has warranted the urgent need to find a cost-effective approach to kill bacteria and viruses on different surfaces for extended periods.

Antimicrobial spray coatings hold great promise in this regard as they are easy-to-apply coatings, a layer of which can be sprayed on surfaces to impart a sustained antimicrobial effect. Since disinfectant application will be required less frequently, both cost of disinfection and the possibility of developing bacterial resistance will be minimized. In addition, the antimicrobial effect would be effective for a specific time range, so unintended failure to apply a disinfectant will not lead to a risk of cross-contamination.

Surface coatings with nanoparticles (NPs) embedded with antimicrobial agents have been developed by different groups.[3–5] For instance, Kruk *et al.*[6] reported the utilization of silver NPs, as an antimicrobial agent, encapsulated in polyelectrolyte film as an effective antibacterial coating. In addition, Ma *et al.*[7] introduced a green method for the synthesis of monodisperse, small size silver NPs that were stabilized with soluble soybean polysaccharide as effective antibacterial coatings. The size of the nanoparticles plays an important role in antimicrobial activity. The high surface-to-volume ratio enables them to better interact and fuse with the bacterial cell membranes.[8] Most of the nanoparticles containing antimicrobial agents were made using silver NPs. Continuous exposure to silver NPs has been proven to cause toxicity,[5,9,10] which may limit the long-term application of such coatings. In addition, the cost of raw materials and/or production procedures of these coatings may not be suitable for large scale applications. Alternatively, other types of NPs may be better tolerated, and can be synthesized at a lower production cost (hence with better scalability), without compromising the desired antimicrobial activity.

[a]*Department of Chemistry, School of Sciences and Engineering, The American University in Cairo, New Cairo, Cairo 11835, Egypt. E-mail: hazzazy@aucegypt.edu; wesamawad@aucegypt.edu*

[b]*Department of Nanobiophotonics, Leibniz Institute of Photonic Technology, Jena, 07745 Germany*

† Electronic supplementary information (ESI) available. See DOI: https://doi.org/10.1039/d2na00950a

© 2023 The Author(s). Published by the Royal Society of Chemistry

Open Access Article. Published on 21 March 2023. Downloaded on 2/11/2026 2:45:44 PM. This article is licensed under a Creative Commons Attribution-NonCommercial 3.0 Unported Licence.

Polymethylmethacrylate polymer (PMMA) is a transparent polymer with low toxicity as it does not contain harmful subunits.[11] Moreover, this polymer exerts antimicrobial activity which leads to a desirable synergistic effect with the embedded antimicrobial materials.[12] Furthermore, it has antifouling properties resulting in less accumulation of dirt on its surface, which, in combination with the transparent nature of PMMA, would lead to an elegant appearance after surface coating.[13] The antimicrobial activity of the PMMA NPs with net positive charge stems from the simulation of the general chemical structure of the naturally occurring antimicrobial peptides. The synthetic polymers are gifted with an intrinsic antimicrobial activity by the presence of hydrophobic moieties in the polymer chain. While the microbial membrane penetration is facilitated by the hydrophobic parts, the interaction of the NPs with the bacterial cell walls, known to be negatively charged, is enabled by its overall cationic charge.[14]

Benzoyl peroxide (BPO) exhibits versatile modes of action against microbial agents hence making it impervious to bacterial resistance.[15] The antimicrobial activity of BPO is attributed to the free radicals generated by the degradation of BPO, which cause damage to the microbial cell wall and cytoplasmic membrane.[16] Moreover, BPO has been reported to have potent antibacterial activities against resistant bacterial strains.[17]

Benzalkonium chloride (BKC) is a positive biocidal agent with broad-spectrum antimicrobial activities.[18,19] BKC's bactericidal efficacy has been associated with the alternation of microbial membrane permeability, that is followed by dissociation of the microbial cellular membrane, causing cytolytic leakage of the cellular content.[20]

In this work, different nanoformulation approaches for encapsulating BPO and BKC were investigated including nanoprecipitation and emulsification as well as polymer-free nanomicelle synthesis, in order to identify the most cost-effective scalable method for the synthesis of stable nanoparticles for use as nanoparticle-based antimicrobial spray coatings (NBASC) that can be applied on surfaces for a prolonged antimicrobial effect.

Materials and methods

Materials

Polymethylmethacrylate (PMMA) polymer (molecular weight: 400 000 to 550 000 kDa) was purchased from Alfa Aesar (Kandel, Germany). Benzoyl peroxide (BPO), benzalkonium chloride (BKC), acetone, and dimethylsulfoxide (DMSO) were purchased from Loba Chemie (Mumbai, India). Sodium dodecylsulfate and Triton X-100 (TX-100) were acquired from Serva (Heidelberg, Germany). Tween 80 was supplied by Adwic Company (Cairo, Egypt). Dichloromethane (DCM) was acquired from Carlo-Erba (Milan, Italy). Distilled water (DW) was used in all experiments. RPMI 1640 was obtained from Corning (NYC, USA), and Fetal Bovine Serum was obtained from High-Sense (PA, USA). Penicillin–streptomycin (10×), L-glutamine, and trypsin (0.025%) were obtained from Lonza (Basel, Switzerland). Phosphate buffered saline (PBS, pH 7.4) was obtained from Genetix Biotech (New Delhi, India) and 3-(4,5-dimethylthiazol-2-yl)-2,5-diphenyltetrazolium bromide (MTT) was obtained from SERVA (Heidelberg, Germany). Nutrient broth was obtained from NEOGEN (Lansing, MI, USA). Agar–Agar was obtained from B&V (Parma, Italy).

Methods

Synthesis of polymeric PMMA nanoparticles

Nanoprecipitation by the solvent-shifting technique. Nanoprecipitation by solvent-shifting was performed in water using a miscible organic solvent (acetone). The hydrophobic polymer (PMMA) and the active ingredient (BPO) were first dissolved in a polar solvent that is fully miscible with water.[21] Different trials were carried out for the synthesis of PMMA NPs as follows: three different concentrations (0.2%, 0.4%, and 0.8%) of PMMA were first dissolved in acetone, separately. Second, an aqueous solution of a surfactant (1% TX-100 in DW) was prepared. The acetone solution was then added dropwise to the aqueous solution at an organic:aqueous ratio of 1 : 5.

Because PMMA precipitated in all the formulas (without the formation of NPs), preparation of NPs using this technique was not considered. The constituents of each phase in all the trials of prepared nanoprecipitation (NPT) formulas are presented in Table 1.

Synthesis via the emulsification-solvent evaporation technique. The emulsification-solvent evaporation method consists of two main steps: emulsification, followed by organic solvent evaporation, leaving a surfactant-stabilized polymer colloid loaded with active components.[22] This technique is suitable for entrapment of hydrophobic active agents resulting in high encapsulation efficiency. Here, the organic phase was formed by dissolving 1% PMMA and 1% BPO separately in dichloromethane (DCM). On the other hand, the aqueous phase contained a binary surfactant mixture (except in the first trial). The used surfactants were Triton X-100 (TX-100) and BKC. Subsequently, the two DCM solutions (containing 1% PMMA or 1% BPO) were mixed in a 1 : 1 ratio then added, dropwise, to the aqueous solution (in various ratios) with vigorous mechanical stirring. After addition, the mechanical stirring was carried on for an additional 5 min. Subsequently, the organic solvent was

Table 1 Compositions of the fabricated nanoprecipitation (NPT) formulas

Formula	Lipophilic constituents	Hydrophilic constituents	Volume ratio (org : aq)	Surfactant
NPT-1	0.2% PMMA in acetone	1% TX-100 in DW	1 : 5	Tween 80
NPT-2	0.4% PMMA in acetone	1% TX-100 in DW	1 : 5	Tween 80
NPT-3	0.8% PMMA in acetone	1% TX-100 in DW	1 : 5	TX-100

© 2023 The Author(s). Published by the Royal Society of Chemistry

Open Access Article. Published on 21 March 2023. Downloaded on 2/11/2026 2:45:44 PM. This article is licensed under a Creative Commons Attribution-NonCommercial 3.0 Unported Licence.

Table 2 Nanoparticle formulas prepared *via* the emulsification-solvent evaporation method

Formula	Lipophilic constituents	Hydrophilic constituents	Volume ratio (org : aq)	Surfactants
NE-1	0.2% PMMA + 0.2% BPO in DCM	2% BKC + 1% TX-100 in DW	1 : 5	BKC + TX-100
NE-2	0.4% PMMA + 0.4% BPO in DCM	2% BKC + 1% TX-100 in DW	1 : 5	BKC + TX-100
NE-3	0.8% PMMA + 0.8% BPO in DCM	2% BKC + 1% TX-100 in DW	1 : 5	BKC + TX-100

left to evaporate, overnight, by constant stirring at room temperature. Meanwhile, evaporation of the organic solvent was followed by precipitation of the polymer encapsulating the drug as NPs. The constituents of each phase are presented in Table 2.

Synthesis of polymer-free nanomicelles. The nanomicelle (NM) preparation trials were performed *via* the solvent evaporation method previously reported by You *et al.* in 2021,[23] with some modifications. Briefly, different concentrations of BPO (0.2%, 0.4%, or 0.8%) were dissolved in acetone to obtain the organic phase. Separately, the aqueous phase was prepared using a surfactant mixture, 2% BKC and 1% TX-100. The organic phase was addeddropwise to the aqueous phase with magnetic stirring (at 800 rpm) and left stirring overnight to allow complete evaporation of acetone. The constituents of each phase are reported in Table 3.

Physicochemical characterization of the prepared nanoparticles

Particle size and zeta potential measurements. The average particle size and size distribution of the prepared nanoparticles were measured by Dynamic Light Scattering (DLS) utilizing a Malvern Zetasizer Nano ZS90 (Malvern Instruments, Worcestershire, UK) equipped with a 10 mW He–Ne laser (633 nm) and operating at an angle of 90° and a temperature of 25°C. The samples were diluted 1 : 20 with distilled water, pipetted into a disposable plastic cuvette, and measured in triplicate. Zeta potential distribution was measured for the same samples with zeta limits of −120 to 120 V.

Fourier-transform infrared spectroscopy (FTIR). The FTIR spectra of the prepared PMMA NPs and nanomicelle colloids were obtained using FTIR Spectroscopy using a Nicolet 380 spectrometer (ThermoScientific Nicolet, Waltham, MA), and the spectra were recorded in the range of 4000–500 cm^{-1}, at a resolution of 4 cm^{-1}. The colloids were pressed between two plates of a KBr (FTIR) Liquid Cell, before characterization. BPO and PMMA were characterized as well, after being mixed with ground KBr and compressed into disks.

High resolution transmission electron microscopy (HRTEM). The nanoparticles' morphology and particle size distribution were studied using HRTEM imaging and image analysis. Aliquots of the prepared PMMA NPs and nanomicelle colloids were stained with 2% aqueous phosphotungstic acid. The mixtures were added dropwise and dried over carbon-coated copper 200 mesh grids to be photographed. HRTEM was performed using a JEOL-JEM 2100 electron microscope (Musashino, Akishima, Tokyo, Japan), operating at 160 kV. To obtain the particle diameter histograms, direct images were analyzed using the image processing software ImageJ (NIH, Bethesda, MD, USA). The particle diameter (nm) was averaged from a total of 150 measurements for each sample. In addition, the selected area electron diffraction (SAED) patterns were obtained by using the transmitted and one of the diffracted beams.

Stability testing. The assessment of the long-term stability is essential when developing a new nanoparticle system as it shows its suitability for commercial application. Long-term stability testing has been performed for the prepared PMMA NPs and nanomicelles for 9 months. The samples were stored in well-sealed containers, at room temperature to mimic the storage of the spray coatings on shelf.[24,25] After 9 months, the stability of the nanoparticle colloids was investigated in terms of particle size, size distribution, and morphology (*via* HRTEM imaging and image analysis). In addition, measurement of the antibacterial activity of the NPs was repeated to ensure that they retained their antibacterial properties.[26]

Biological characterization of the antimicrobial nanoparticle surface coatings

Antibacterial assay. For the disk diffusion method, the prepared NM-3/NE-3 solutions (1 mL each) were aspirated in 1.5 mL Eppendorf tubes and sterilized filter discs of 5.5 mm diameter were added and soaked for 2 h. The controls were 1% Triton X-100, acetone, and the as-prepared NM3 and NE3 without BPO. Afterward, the soaked filter discs were placed on agar Petri dishes spread with 100 μL of 1×10^8 cells per mL (log 8 mL^{-1}) of bacterial strains *P. aeruginosa*, *S. aureus*, or *E. coli*. The Petri dishes were incubated at 37 °C for 18–24 h to measure the inhibition diameter. All samples were measured in triplicate ($n = 3$).

The antibacterial testing of the prepared NM-3/NE-3 was first done on glass surfaces according to an ISO: 22196:2011

Table 3 Preparation of different nanomicelle (NM) formulas

Formula	Lipophilic constituents	Hydrophilic constituents	Volume ratio (org : aq)	Surfactants
NM-1	0.2% BPO in acetone	2% BKC + 1% TX-100 in DW	1 : 5	BKC + TX-100
NM-2	0.4% BPO in acetone	2% BKC + 1% TX-100 in DW	1 : 5	BKC + TX-100
NM-3	0.8% BPO in acetone	2% BKC + 1% TX-100 in DW	1 : 5	BKC + TX-100

Open Access Article. Published on 21 March 2023. Downloaded on 2/11/2026 2:45:44 PM. This article is licensed under a Creative Commons Attribution-NonCommercial 3.0 Unported Licence.

protocol. Briefly, glass surfaces were sterilized by baking at 180 °C for 2 h and used throughout any surface experiment. Then, the surfaces were coated with 100 μL of the prepared NM/NE and left to dry under aseptic conditions. 50 μL of bacterial inoculum (*Pseudomonas aeruginosa*, *Staphylococcus aureus*, or *Escherichia coli*) of log 5.7 bacterial cells was placed on the dry surface and a thin parafilm was placed on top of the inoculum and left for 0 or 24 h. Afterwards, the glass slides were placed in 50 mL Falcon tubes with 10 mL of saline solution (0.9% NaCl) and shaken for 30 s. This procedure was applied for all antimicrobial tests of coated surfaces. The uncoated glass slides served as negative controls to the assay.

A colony forming assay was subsequently conducted to visualize colonies where 100 μL of suspension was spread over sterile nutrient agar (with 0 or 1 : 10 dilutions for test samples, and 1 : 1000 and 1 : 10000 dilutions for negative controls). The inoculated agar plates were placed in the incubator for 24 h and colonies counted the next day. Colony forming units per mL were calculated using eqn (1):

$$\text{CFU per mL} = \text{colony count} \times \text{dilution factor} \times 10 \quad (1)$$

For stability testing of the dried antimicrobial coat, it was left on the glass surface for 0, 24, and 72 h, and 7, 14, 21, 28, 35, and 42 days before applying the bacterial inoculum.

For the tolerability test, glass slides were coated with the as-prepared NM-3 and left to dry under aseptic conditions and inoculated with bacteria and left for 24 h. Then they were reinoculated with bacteria and left for another 24 h. Then NM-3 coated glass slides were washed with saline which was spread over sterile agar for the colony counting assay. The uncoated glass slides were treated as the negative control.

For testing the antibacterial activity upon contact, 100 μL of log 8 mL^{-1} of bacterial inoculum was spread on a sterile agar. Then a sterile glass surface coated with NM-3 was printed on top of the agar for a few seconds and left for 24 h to visualize any formed microbial colonies within the printed area.

For testing on other non-porous surfaces such as metals, a stainless-steel metal was used with the same dimensions as the glass slide and the disinfecting coat was tested for its stability on the steel surface for 4 weeks. The uncoated stainless-steel was treated as the negative control.

Antiviral assay. Infectious bronchitis virus which infects and impedes development of chick embryos was utilized as a model to assess the antiviral activity upon contact with the prepared nanomicelles. The ISO 21702 protocol was followed, which is similar to the antibacterial assay above, but the virus contact with the surface didn't exceed 30 min. The dry coated surface was inoculated with 200 μL of Embryo infective dose 50 (EID_{50}) of 10^7 viral titer per mL of growth medium (DMEM and 10% FBS) and left for 30 min at room temperature under aseptic conditions. The virus on the coated surface was reconstituted in 5 mL PBS and 100 μL was injected into a chick embryo egg which was then incubated for 5 days. On the fifth day, the egg was broken, and the chick embryo was observed regarding its appearance. If dwarfing was observed, it indicated viral activity and ineffectiveness of the antimicrobial coat.[27,28] The uncoated glass slides were treated as the negative control. The number of eggs used were three replicates for each group (NM-3 and control) for each week (1st week, 4th week and 7th week). The results obtained were either dwarfed (−) or normal development (+) for each egg and tabulated.

Cytotoxicity assay. The dry coat (antimicrobial spray) on the sterile glass slide was rubbed with a sterile cotton swab and reconstituted in 1 mL of complete growth medium (RPMI 1640 medium supplemented with 10% FBS, 1× streptomycin–penicillin, and 1× L-glutamine). L929 cells were incubated in 96 well plates at a cell density of 10 000 cells per mL. The reconstituted medium was added to the medium after cell attachment. The cells were incubated at 37 °C and 5% CO_2 for 24 h. 10 μL MTT (5 mg mL^{-1}) were then added to each well and wells were incubated in the dark for 3 h. Liquids in the wells were aspirated and 100 μL of DMSO was added to each well to dissolve the formazan salt. The plates were left to incubate in the dark for 10 min before measuring absorbance at 570 nm using a FLUOstar Omega microplate reader (BMG Labtech, Ortenberg, Germany).

Results and discussion

Physicochemical characterization of the prepared nanoparticles

To achieve nanoparticles exhibiting antimicrobial properties, different fabrication methods were tested including nanoprecipitation by the solvent-shifting technique, emulsification-solvent evaporation technique, and polymer-free nanomicelles.

Three formulas (NPT 1–3) were prepared using the nanoprecipitation technique, however, nanoprecipitation was not effective in generating stable nanoparticles. Clear precipitates were observed just after complete evaporation of the organic solvent. This could be attributed to the rapid diffusion of the organic solvent to the aqueous phase that led to the formation of aggregates and subsequent precipitation.[4,9]

The emulsification-solvent evaporation technique on the other hand was utilized to prepare three formulas (NE 1–3) which resulted in a substantial enhancement in the type of the nanoparticles produced in terms of particle size, charge, and PDI (Table 4). In this approach the immiscible organic solvent forms nanodroplets under intensive homogenization that are coated by a layer of the stabilizer. Afterwards, the organic solvent is slowly evaporated, and stable nanoparticles are formed.

In the nanomicelle technique, three formulas were also prepared (NM 1–3). The elimination of the PMMA polymer

Table 4 Particle size, polydispersity index (PDI), and zeta potential of the prepared nanoemulsion (NE) formulas

Formula	Particle size (nm)	PDI	Zeta potential (mV)
NE-1	856.4	0.733	33
NE-2	557.13	0.606	24
NE-3	24.12	0.4903	50.07

© 2023 The Author(s). Published by the Royal Society of Chemistry

Open Access Article. Published on 21 March 2023. Downloaded on 2/11/2026 2:45:44 PM. This article is licensed under a Creative Commons Attribution-NonCommercial 3.0 Unported Licence.

Table 5 Particle size, polydispersity index (PDI), and zeta potential of the prepared polymer-free nanomicelles (NM)

Formula	Particle size (nm)	PDI	Zeta potential (mV)
NM-1	976.7	1	31.63
NM-2	2240	0.55	18.2
NM-3	72.67	0.1977	46.5

substantially enhanced the stability of the prepared nanomicelles. In this approach, the formation of the nanomicelles solely depended on the self-assembly of the surfactant which acted as a carrier for the hydrophobic content, thus resulting in monodisperse stable nanomicelles as supported by the particle size and zeta potential measurements (Table 5). The third formula (NM-3) displayed the best redispersibility and long-term stability due to its uniform particle size and high surface charge. Removal of the PMMA polymer substantially reduced the cost. In addition, the process itself required less energy consumption due to the usage of low shear mixing speed. The attempts to prepare NMs with BKC only resulted in instant precipitation of the BPO. The utilization of TX-100 as a cosurfactant alongside BKC gave the optimum size distribution and redispersibility. Consequently, NM-3 was selected for further investigations.

Fourier-transform infrared spectroscopy (FTIR) for the NM-3 and NE-3 NPs. FTIR characterization of the prepared NE-3 NPs revealed 3 peaks (Fig. 1) at 1454.69, 1240.12, and 703.69 cm^{-1} that can be attributed to the molecular structure of BPO which consists of two benzoyl groups linked *via* a peroxide (the corresponding peaks in the BPO spectrum were found at 1453.13, 1234.67, and 702.13 cm^{-1}, respectively).[29] In addition, 5 peaks can be attributed to PMMA: the peak found at 1731.45 cm^{-1} corresponds to the C=O stretching vibration of ester groups, the two peaks found at 1383.94 and 734.01 cm^{-1} are due to the α-methyl group vibrations,[30] and the two bands at 1192.69 and 1114.95 cm^{-1} can possibly be attributed to the C–O stretching vibrations of ester groups.[31] The corresponding peaks in the PMMA spectrum were found at 1728.34, 1387.55, 736.17, 1199.69, and 1114.73 cm^{-1}, respectively. Moreover, the two bands found at 2920.92 and 2849.40 cm^{-1} can be attributed to the characteristic asymmetric and symmetric stretching vibrations of the CH_2 groups in alkylammonium cations of BKC.[32,33] A broad peak was also found at 3433.25 cm^{-1} and can be attributed to the terminal OH group in the oxyethylene chain of TX-100 molecules.[34]

The FTIR spectrum of the prepared NM-3 NPs, presented in Fig. 2, showed an absorption peak at 1756.33 cm^{-1}, which can be attributed to the C=O group of BPO. In addition, 4 peaks which can also be related to BPO appeared at 1454.69, 1230.01, 1000.67, and 702.91 cm^{-1}. The corresponding peaks in the BPO spectrum were found at 1758.66, 1453.13, 1234.67, 996.00, and 702.13 cm^{-1}, respectively. These assignments correspond to previously published data.[29] Moreover, the two bands found at 2927.14 and 2848.62 cm^{-1} can be attributed to the characteristic asymmetric and symmetric stretching vibrations of the CH_2 groups in alkylammonium cations of BKC.[32,33] A broad peak was also found at 3444.14 cm^{-1} and can be attributed to the terminal OH group in the oxyethylene chain of TX-100 molecules.[34]

The wavenumbers of peaks observed in the FTIR spectra of the prepared NE-3 NPs, NM-3 NPs, pure PMMA and pure BPO are presented in Table 6.

High resolution transmission electron microscopy (HRTEM) of the NM-3 and NE-3 formulas. The hollow form of the SAED pattern represents the amorphous nature of the prepared NE-3 (Fig. 3a) and NM-3 formulas (Fig. 3b),[35] while the HRTEM micrograph of the NE-3 showed spherical particles (Fig. 4) with particle diameter ranging from 31.91 to 76.12 nm, and an average particle diameter of 52.67 nm (±11.56 nm). The HRTEM micrograph of the NM-3 displayed spherical particles as well (Fig. 5) with particle diameter ranging from 24.28 to 66.37 nm and an average particle diameter of 39.59 nm (±9.27 nm).

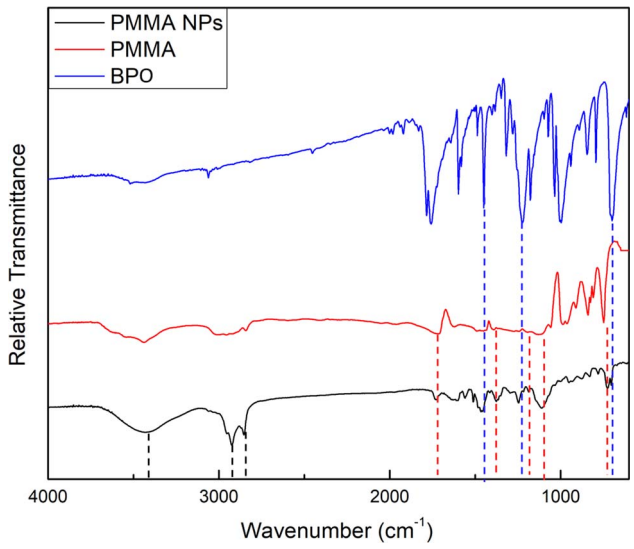

Fig. 1 FTIR spectra of the prepared NE-3 NPs, pure PMMA and pure BPO.

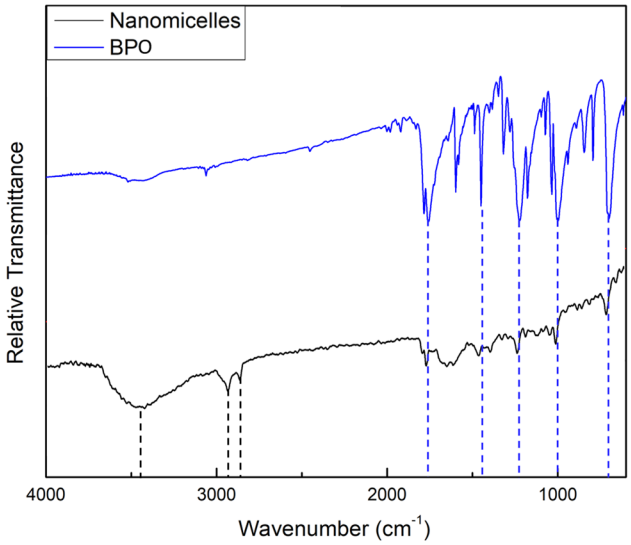

Fig. 2 FTIR spectra of the prepared NM-3 NPs and pure BPO.

© 2023 The Author(s). Published by the Royal Society of Chemistry

Open Access Article. Published on 21 March 2023. Downloaded on 2/11/2026 2:45:44 PM. This article is licensed under a Creative Commons Attribution-NonCommercial 3.0 Unported Licence.

Table 6 Wavenumbers of peaks observed in the FTIR spectra of the prepared NE-3 NPs, NM-3 NPs, pure PMMA and pure BPO

Chemical compound		Functional group vibration	Wavenumber (cm^{-1})	Ref.
Pure BPO		C=O vibration	1758.66	29
		C=C vibration	1453.13	
		C–O asymmetric stretching	1234.67	
		C–O symmetric stretching	996.00	
		C-H out-of-plane bending	702.13	
Pure PMMA		C=O of ester group stretching vibration	1728.34	30
		α-Methyl group vibration	1387.55	
			736.17	
		C–O stretching vibrations of ester groups	1199.69	31
			1114.73	
NE-3 NPs	BPO	C=C vibration	1454.69	29
		C–O asymmetric stretching	1240.12	
		C–H out-of-plane bending	703.69	
	PMMA	C=O of ester group stretching vibration	1731.45	30
		α-Methyl group vibration	1383.94	
			734.01	
		C–O stretching vibrations of ester groups	1192.69	31
			1114.95	
	BKC	Asymmetric and symmetric stretching vibrations of the CH_2 groups in alkylammonium cations	2920.92	32 and 33
			2849.40	
	TX-100	Terminal OH group in the oxyethylene chain	3433.25	34
NM-3 NPs	BPO	C=O vibration	1756.33	29
		C=C vibration	1454.69	
		C–O asymmetric stretching	1230.01	
		C–O symmetric stretching	1000.67	
		C–H out-of-plane bending	702.91	
	BKC	Asymmetric and symmetric stretching vibrations of the CH_2 groups in alkylammonium cations	2927.14	32 and 33
			2848.62	
	TX-100	Terminal OH group in the oxyethylene chain	3444.14	34

Stability test

High resolution transmission electron microscopy (HRTEM). After 9 months of storage at room temperature, the NM-3 and NE-3 showed comparable stability as evidenced from their particle size and surface charge data (Fig. 6 and 7). The particle diameter ranges from 16.29 to 63.76 nm, with an average diameter of 34.12 nm (±10.34 nm). Similarly, the HRTEM micrograph of the NM-3 NPs revealed that the particles retained their spherical shape as well (as presented in Fig. 7) with particle diameter ranging from 20.78 to 76.05 nm, and an average diameter of 39.01 nm (±11.56 nm). Hence, the particle size, size distribution, and morphology of the prepared NE-3

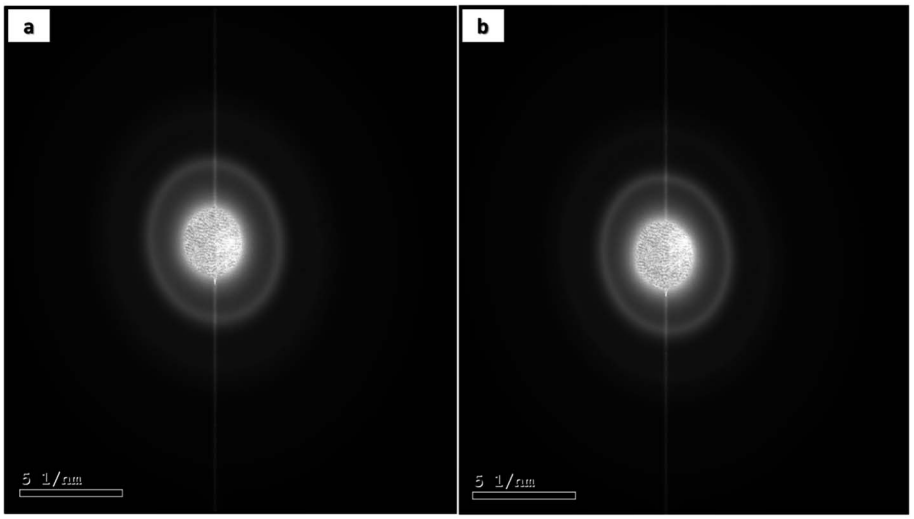

Fig. 3 SAED patterns of the prepared NE-3 (a) and NM-3 (b).

 © 2023 The Author(s). Published by the Royal Society of Chemistry

Open Access Article. Published on 21 March 2023. Downloaded on 2/11/2026 2:45:44 PM.
This article is licensed under a Creative Commons Attribution-NonCommercial 3.0 Unported Licence.

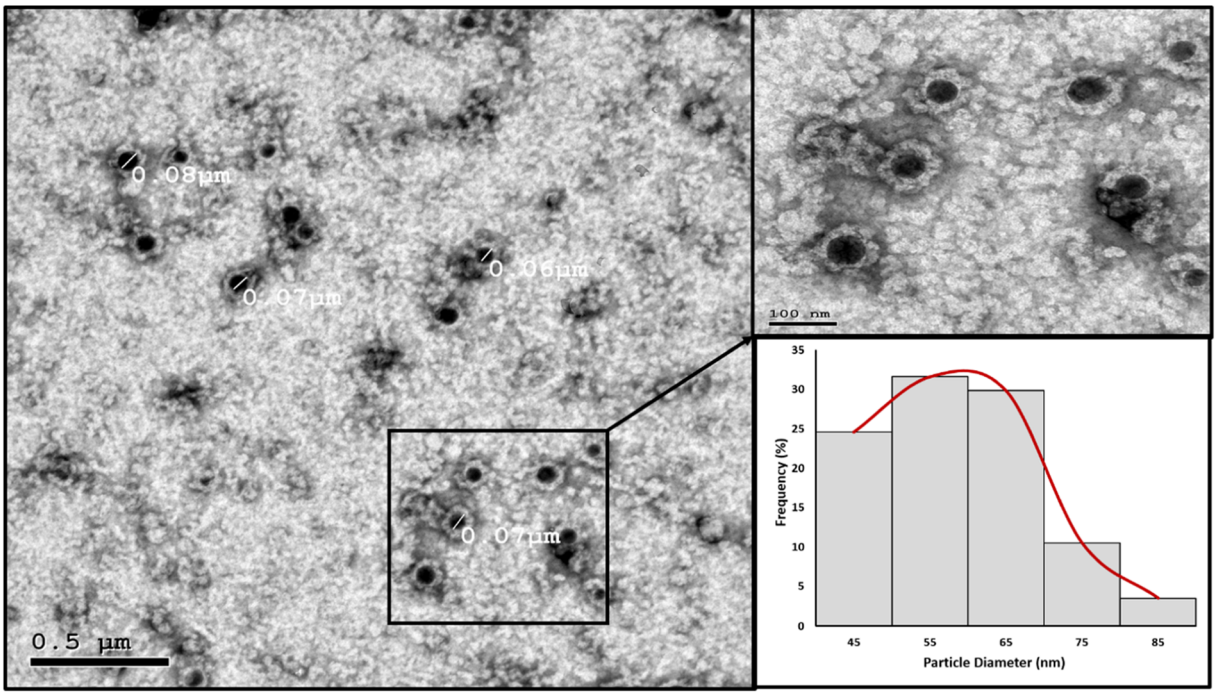

Fig. 4 HRTEM image and particle diameter (nm) distribution histogram of the prepared NE-3.

and NM-3 were stable over 9 months of storage at room temperature.

Biological characterization of the prepared nanoparticles

Disk diffusion assay. NM-3 and NE-3 containing BPO and BKC were tested for their antibacterial activity using the disc diffusion method. As shown in Fig. 8, NM-3 and NE-3 have similar inhibition zones of disk diffusion method across all strains of bacteria (*P. aeruginosa*, *E. coli*, and *S. aureus*). On the other hand, BPO (0.2%) had little effect on *E. coli* but no antibacterial activity on *P. aeruginosa* and *S. aureus*. Though the disc filter papers were incubated with BPO in acetone for 48 h (Fig. 8,

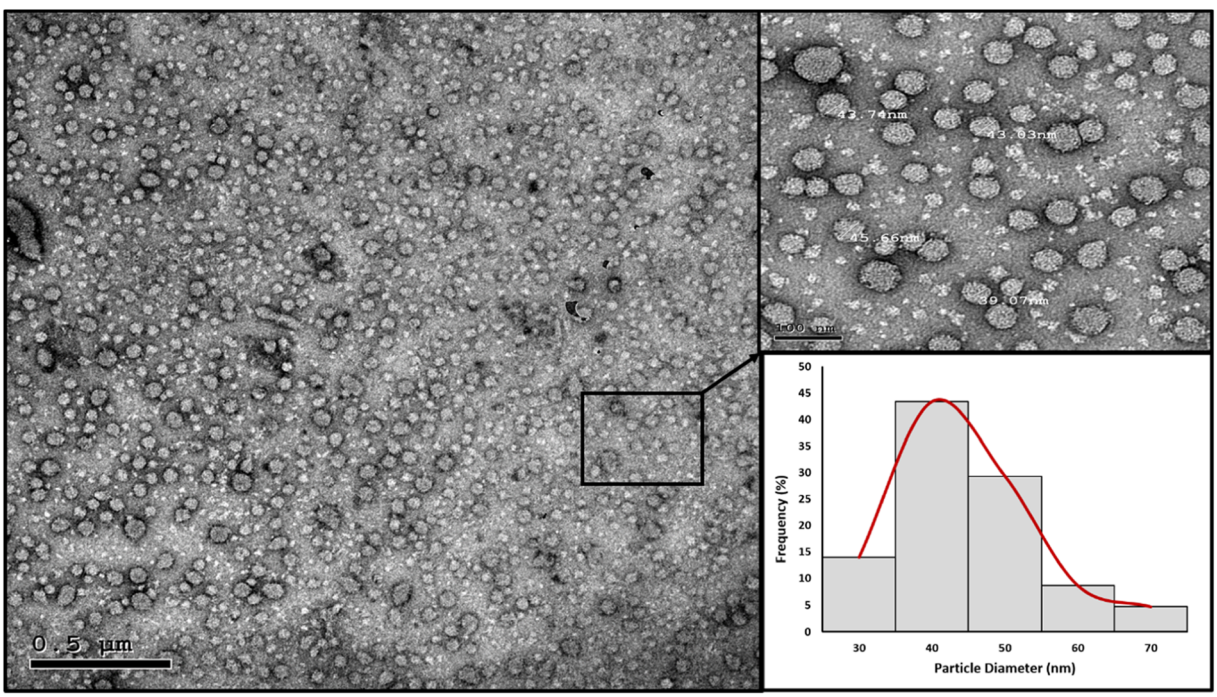

Fig. 5 HRTEM image and particle diameter (nm) distribution histogram of the prepared NM-3.

Open Access Article. Published on 21 March 2023. Downloaded on 2/11/2026 2:45:44 PM.
This article is licensed under a Creative Commons Attribution-NonCommercial 3.0 Unported Licence.

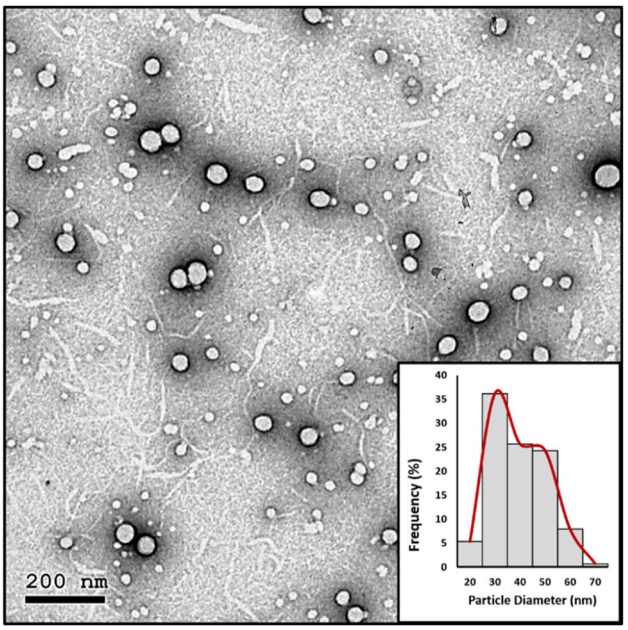

Fig. 6 HRTEM image and particle diameter (nm) distribution histogram of the prepared NE-3 NPs after 9 months of storage at room temperature.

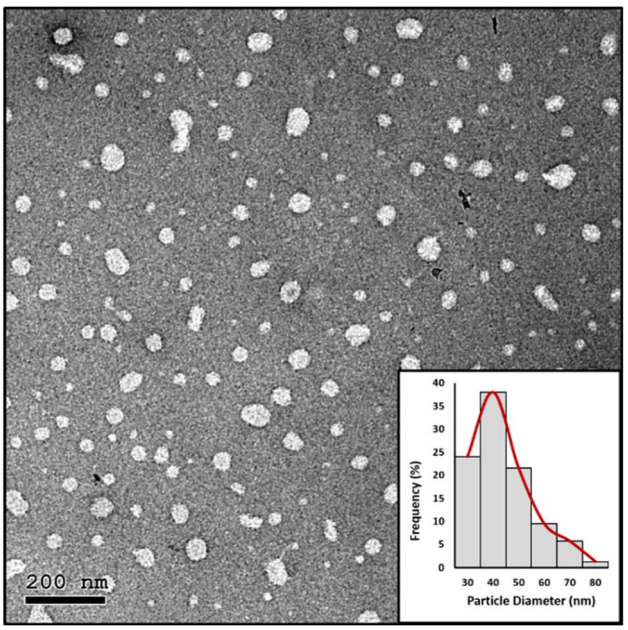

Fig. 7 HRTEM image and particle diameter (nm) distribution histogram of the prepared nanomicelles (NM-3 NPs) after 9 months of storage at room temperature.

disk number 4). Activation of BPO requires some absorption to the cellular membrane and interaction with reactive oxygen species to break the peroxide bond and produce free radicals.[15,17,36–39] Also, the disc diffusion assay of BPO dissolved in TX-100 did not show any antibacterial activity. Also, 1% TX-100 alone did not show antibacterial activity (ESI Fig. 1†). Moreover, the NM3/NE3 without BPO showed similar inhibition diameters in Fig. 8 (ESI Fig. 1†). Therefore, the observed antibacterial effect was caused by BKC which has IC_{50} of 0.01% for *E. coli* and *S. aureus*, and 0.1% for *P. aeruginosa* (ESI Table 1†). Since NM-3 showed enhanced stability as compared to NE-3 (Tables 4 and 5), NM-3 was selected for further investigations of the antibacterial/antiviral activities.

Antibacterial testing of NM-3

To demonstrate the antibacterial activity of NM-3 (which contains BPO as the core and BKC as the coat) upon surface contact a method is used that mimics microbial contamination of public surfaces such as doorknobs, tables, rails, *etc.*[37,40,41] The simplest method was to use glass slides as a non-porous surface that is easy to autoclave and preserves its sterility until experimentation. The coat was always allowed to dry under aseptic conditions. The number of bacteria added was 50 μL of log 5.7 bacteria/slide which is the maximum reported bacterial density on surfaces used by the public.[40] Finally, to enumerate the amount bacteria that survived, normal saline was used, as the transfer media, and a negative control (uncoated glass slide) was used to enumerate the number of colonies that survived on the sterile slide without NM-3.[40] The negative controls showed 2.8×10^6 cells per mL for *P. aeruginosa*, 1.67×10^6 cells per mL for *S. aureus* and 6.4×10^6 cells per mL for *E. coli*. Results showed that the NM-3 have a potent and persistent antibacterial activity. The dried NM-3 coat on glass slides was left for 5 min and 24 h, after which no bacterial colonies were detected. Moreover, to test the NM-3 for prolonged antibacterial activity, the slides were left for 3, 4, and 7 days and then 2, 3, 4, 5, 6 and 7 weeks (Fig. 9). Bacteria were inoculated at each time point and enumerated as presented in Fig. 9 (ESI Fig. 2† shows week 3). This confirms the stability of the NM-3 and its antibacterial activity over a long period.

The nanomaterial's tolerability has been demonstrated which simulates a situation which may occur on high traffic surfaces. NM-3 coated glass slides were inoculated several times (2–3) followed by testing the ability of the coating with the antimicrobial coat (which was applied once to the surface) to neutralize the repeated bacterial contamination. As shown in Fig. 10B, the NM-3 dry coat still showed antibacterial activity although it was inoculated twice the normal bacterial inoculum in succession. So typically, the developed formula would disinfect surfaces which are not frequently washed for extended periods.

To address the NM-3 capability of antibacterial activity upon contact, the coated glass slides were simply printed onto the agar (that is spread with the different bacterial strains) followed by incubation for 24 h.[41] As shown in Fig. 10C, the inhibited zone created by the coated glass slide showed the ability of NM-3 to inhibit antibacterial growth upon contact.

Testing the NM-3 antibacterial effect on a stainless steel surface. The antibacterial effect of NM-3 was assessed on other non-porous surfaces such as stainless steel which is utilized in doorknobs, faucets, and handrails. NM-3 showed similar prolonged antibacterial activities against the three bacterial strains (ESI Fig. 3†).

© 2023 The Author(s). Published by the Royal Society of Chemistry

Open Access Article. Published on 21 March 2023. Downloaded on 2/11/2026 2:45:44 PM.
This article is licensed under a Creative Commons Attribution-NonCommercial 3.0 Unported Licence.

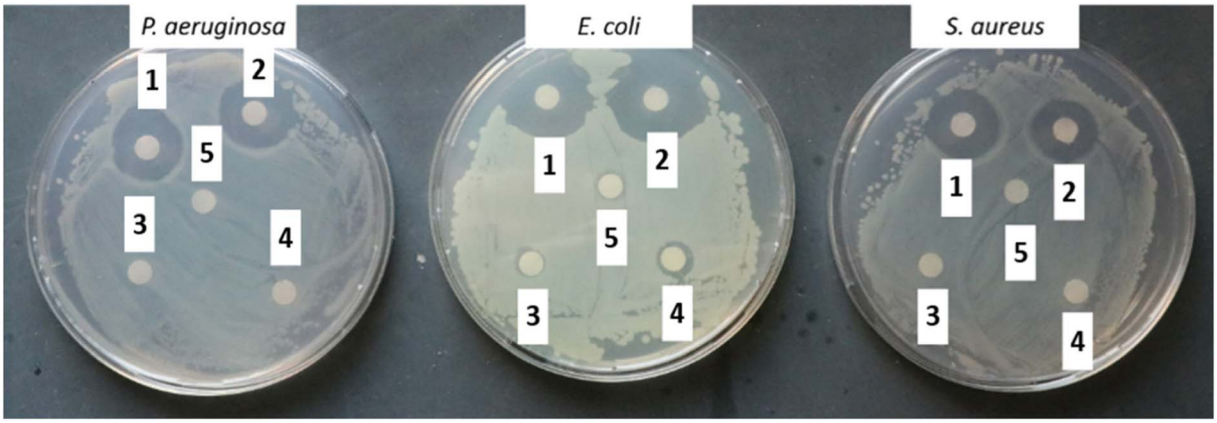

Fig. 8 Disk diffusion method for testing the antibacterial activities of NE-3 (1), NM-3 (2), BPO (3), BPO in acetone for 48 h (4) and acetone (5) against three different bacterial strains.

Testing the NM-3 antiviral activity. The antiviral assay of infectious bronchitis virus (IBV) was done following the ISO 21702 protocol. The glass slides were coated with NM-3, left to dry, inoculated with IBV, left for 30 min, then viral particles were collected in PBS. Afterwards the IBV's virulency was assessed by observing the infected chick embryo after 5 days of incubation. Dwarfing of the infected chick embryo indicates virulent IBV while normal embryonic development indicates antiviral activity of NM-3 against IBV. The NM-3 coated glass slides showed 100% normal development of chick embryos as compared to the control non-coated surfaces where dwarfing occurred. The prolonged antiviral activity of NM-3 was tested where the glass slides were coated with NM-3 and dried for 1, 4 and 7 weeks before inoculation with IBV as described above

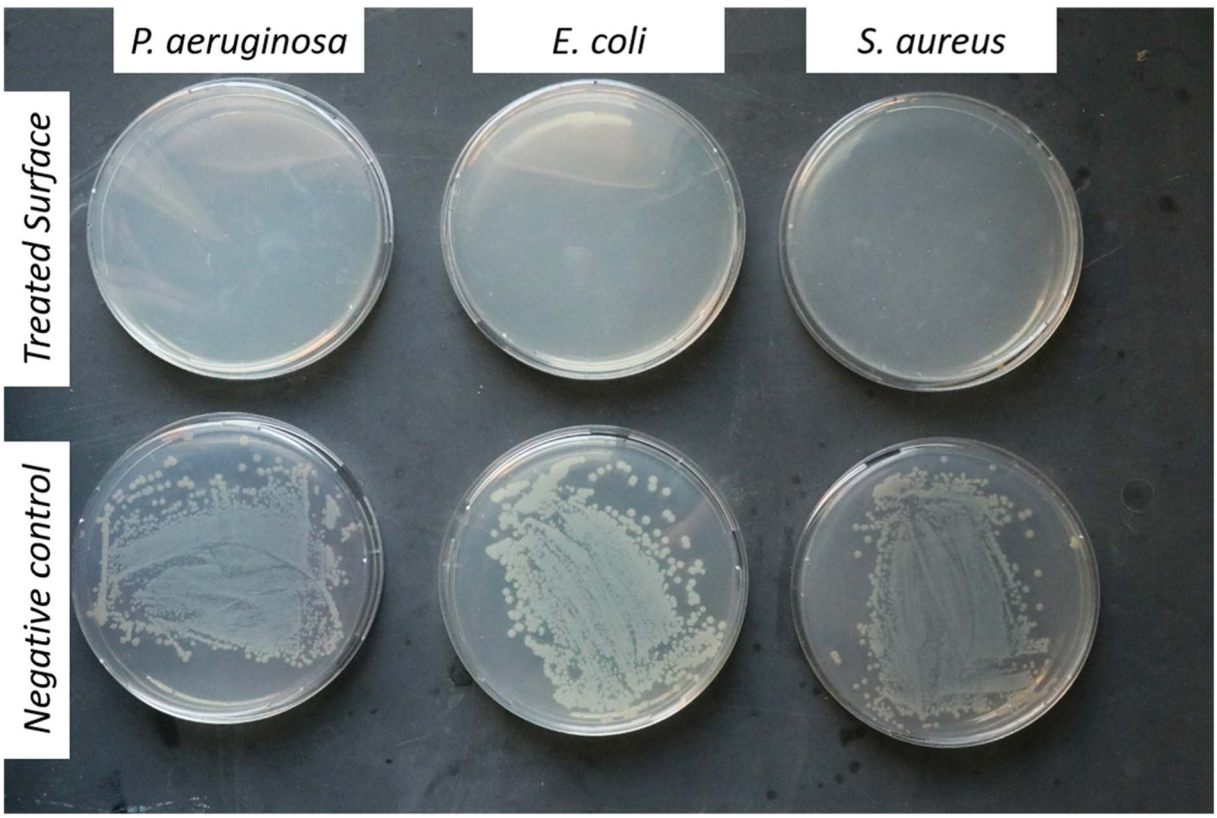

Fig. 9 Colony forming unit assay utilizing surface treatment of NM-3 on three bacterial strains after 7 weeks. In this experiment, glass slides were coated with NM-3, left to dry, then stored under aseptic conditions for 7 weeks. Then slides were inoculated with bacteria and left for 24 h, then reconstituted in saline solution from which 100 μL was plated on sterile agar.

Open Access Article. Published on 21 March 2023. Downloaded on 2/11/2026 2:45:44 PM.
This article is licensed under a Creative Commons Attribution-NonCommercial 3.0 Unported Licence.

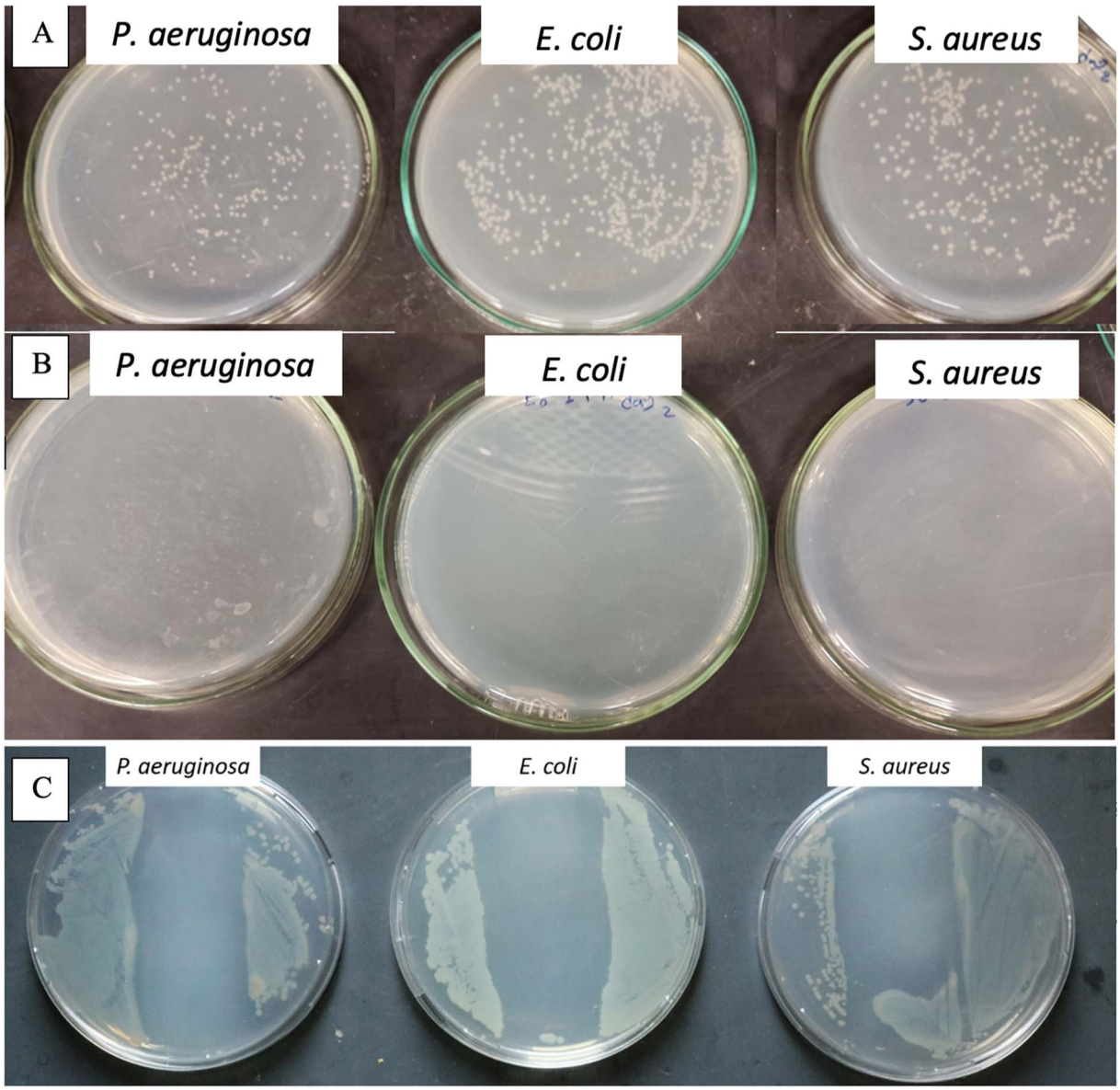

Fig. 10 Antibacterial tests of NM-3. (A) Agar plates treated with uncoated glass slides (negative control). (B) Glass slides coated with NM-3 and left to dry under aseptic conditions, then inoculated with bacteria and left for 24 h and then reinoculated again with bacteria and left for another 24 h. (C) The NM-3 coated surfaces printed on bacterial smear on agar showing antibacterial activity just upon contact.

(Table 7). Because the chick embryos treated with IBV collected from NM-3 coated surfaces showed normal development, this suggests that the virus has been inactivated by NM-3 and lost its virulence. Additionally, NM-3 reconstituted in PBS didn't affect normal development of the chick embryo which indicates no or minimal toxic effect of NM-3.

Table 7 Antiviral assay showing normal development of chick embryo (+) or dwarfing (–) in the presence of viral activity. Experiments were done in triplicate

Samples	Week 1	Week 4	Week 7
NM-3 treated slides	+, +, +	+, +, +	+, +, +
Negative control	–, –,–	–, –, –	–, –, –

Cytotoxicity of NM-3. The cytotoxicity of NM-3 was evaluated using a method similar to the antibacterial assay (ISO: 22196:2011 protocol). 96-well plates were treated with NM-3 and left to dry. Then L929 cells were added into the wells where the color of the medium (red) changed to faint pink/orange indicating a change in the pH of the medium (ESI Fig. 4†). Therefore, another method of measuring cytotoxicity was followed by rubbing the dry coat of NM3 with a sterile cotton swab and soaking it in growth media to test its cytotoxicity. The cytotoxicity test in this manner would shed light on how the NM-3 dry coat would chemically challenge the cells, for example if it comes in contact with the skin. Fig. 11 shows the viability of L929 cells after application of treated media (containing the NM-3 dry coat). The viability of the control group (sterile cotton

© 2023 The Author(s). Published by the Royal Society of Chemistry

Open Access Article. Published on 21 March 2023. Downloaded on 2/11/2026 2:45:44 PM.
This article is licensed under a Creative Commons Attribution-NonCommercial 3.0 Unported Licence.

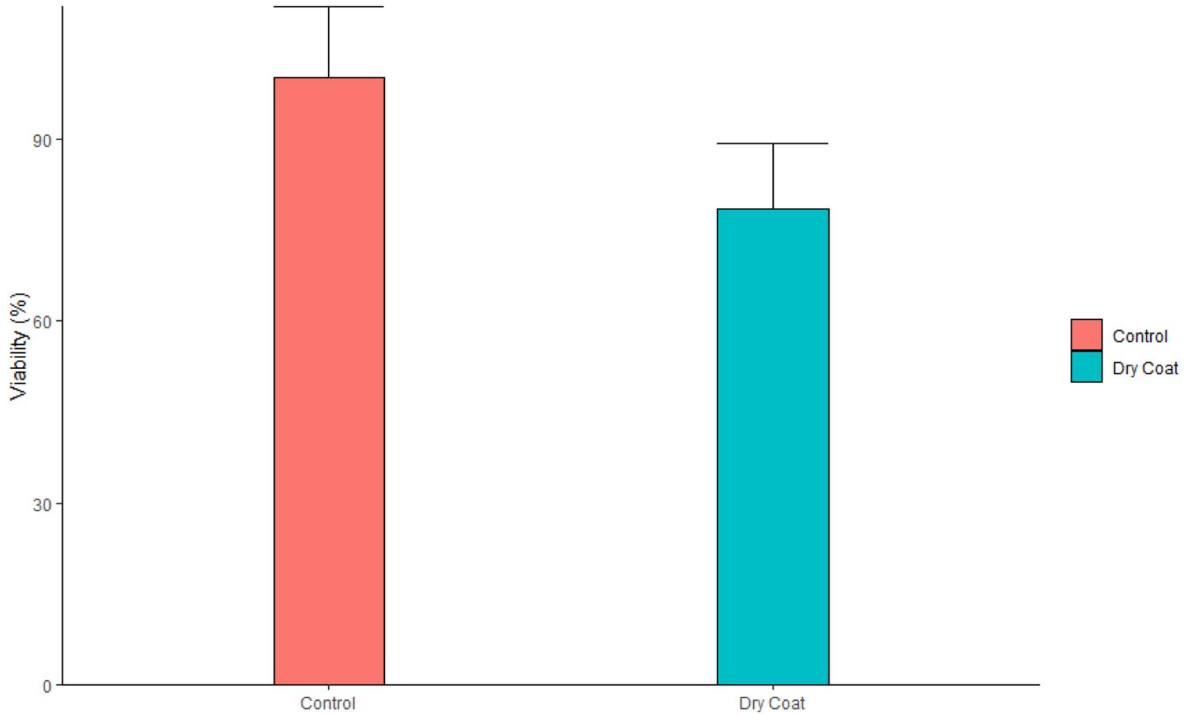

Fig. 11 Viability of the L929 cells against the dry coat of NM-3 that was scrubbed gently with a sterile dry cotton swab which was then soaked in growth medium which was then added to seeded cells in 96-well plates.

swab soaked in growth media) and cells treated with NM-3 dry coat was 100 and 78.4% respectively. The Wilcox rank sum test for unpaired groups indicated that the observed difference is insignificant ($p = 0.2$). Therefore, the NM3 dry coat would be considered safe.

Conclusions

Antimicrobial nanostructures were successfully prepared utilizing two main approaches, the emulsification-solvent evaporation technique and polymer-free nanomicelles. The prepared nanostructures were spherical, with a size of 24.12 nm for NE-3 and 72.67 nm for NM-3; both had a relatively narrow size distribution. They showed high colloidal stability over a span of 9 months which is attributed to their high surface charge. The prepared spray nanostructures containing benzoyl peroxide and benzalkonium chloride exhibited antimicrobial properties against *E. coli*, *S. aureus*, and *P. aeruginosa*. The NM-3 formula consisting of 2% BKC and 1% TX-100 and containing 0.8% BPO displayed the best redispersibility and long-term stability due to its uniform particle size and high surface charge. As compared to other prepared formulas, NM-3 was the least expensive due to removal of PMMA and its preparation required the least energy. Interestingly, a single spray application with NM-3 maintained total inhibition of microbial growth on different surfaces over a period of 7 weeks. Moreover, NM-3 exhibited antiviral properties against IBV. Based on its antiviral/antibacterial properties, the NM-3 nanoformula would be an excellent candidate as a particulate spray for prolonged protection of surfaces against microbial contamination.

Conflicts of interest

Authors are coinventors on a patent application describing the development of nanoparticle formulations containing antimicrobial agents as long acting antimicrobial surface coatings.

Note added after first publication

This article replaces the version published on April 12, 2023, which contained errors in Table 6.

Acknowledgements

This work was funded by a grant from the American university in Cairo to Prof. Hassan M. E. Azzazy. The authors thank Dr Karim Selim and Dr Abdullah Selim from the Reference Laboratory for Quality Control of Poultry Production, Animal Health Research Institute, Agriculture Research Center, Giza, Egypt, for carrying out the antiviral assay.

References

1 M. Saccucci, *et al.*, Surface Disinfections: Present and Future, *J. Nanomater.*, 2018, **2018**, 8950143.
2 Z. Sun and K. Ostrikov, Future antiviral surfaces: Lessons from COVID-19 pandemic, *Sustainable Mater. Technol.*, 2020, **25**, e00203.
3 N. Cioffi, *et al.*, Synthesis, analytical characterization and bioactivity of Ag and Cu nanoparticles embedded in poly-

Open Access Article. Published on 21 March 2023. Downloaded on 2/11/2026 2:45:44 PM. This article is licensed under a Creative Commons Attribution-NonCommercial 3.0 Unported Licence.

vinyl-methyl-ketone films, *Anal. Bioanal. Chem.*, 2005, **382**(8), 1912–1918.
4 A. Fedotova, *et al.*, Packaging materials manufactured from natural polymers modified with silver nanoparticles, *International Polymer Science and Technology*, 2010, **37**(10), 59–64.
5 M. L. Knetsch and L. H. Koole, New strategies in the development of antimicrobial coatings: the example of increasing usage of silver and silver nanoparticles, *Polymers*, 2011, **3**(1), 340–366.
6 T. Kruk, *et al.*, Nanostructured multilayer polyelectrolyte films with silver nanoparticles as antibacterial coatings, *Colloids Surf., B*, 2016, **137**, 158–166.
7 Z. Ma, *et al.*, Green synthesis of silver nanoparticles using soluble soybean polysaccharide and their application in antibacterial coatings, *Int. J. Biol. Macromol.*, 2021, **166**, 567–577.
8 A. Mandal, *et al.*, Synthesis, characterization and comparison of antimicrobial activity of PEG/TritonX-100 capped silver nanoparticles on collagen scaffold, *Colloids Surf., B*, 2012, **90**, 191–196.
9 C. Beer, *et al.*, Toxicity of silver nanoparticles—nanoparticle or silver ion?, *Toxicol. Lett.*, 2012, **208**(3), 286–292.
10 S. Marin, *et al.*, Applications and toxicity of silver nanoparticles: a recent review, *Curr. Top. Med. Chem.*, 2015, **15**(16), 1596–1604.
11 M. I. Ali and K. A. Saleh, Electropolymerization of N-Salicyly tetrahydro phthalamic acid for anticorrosion and antibacterial action applications, *IOP Conference Series: Materials Science and Engineering*, IOP Publishing. 2019.
12 S. Gomez-Carretero, R. Nybom and A. Richter-Dahlfors, Electroenhanced antimicrobial coating based on conjugated polymers with covalently coupled silver nanoparticles prevents Staphylococcus aureus biofilm formation, *Adv. Healthcare Mater.*, 2017, **6**(20), 1700435.
13 V. Kumar, *et al.*, Development of silver nanoparticle loaded antibacterial polymer mesh using plasma polymerization process, *J. Biomed. Mater. Res., Part A*, 2013, **101**(4), 1121–1132.
14 S. J. Lam, *et al.*, Antimicrobial polymeric nanoparticles, *Prog. Polym. Sci.*, 2018, **76**, 40–64.
15 L. H. Kircik, The role of benzoyl peroxide in the new treatment paradigm for acne, *J. Drugs Dermatol.*, 2013, **12**(6), s73–s76.
16 A. J. Friedman, *et al.*, Antimicrobial and Anti-Inflammatory Activity of Chitosan–Alginate Nanoparticles: A Targeted Therapy for Cutaneous Pathogens, *J. Invest. Dermatol.*, 2013, **133**(5), 1231–1239.
17 N. Raytthatha, Development of benzoyl peroxide loaded nanosponges gel, *Nat. J. Pharm. Sci.*, 2021, **1**(2), 25–29.
18 J. T. Walton, *et al.*, Investigation into the effect of detergents on disinfectant susceptibility of attached Escherichia coli and Listeria monocytogenes, *J. Appl. Microbiol.*, 2008, **105**(1), 309–315.
19 R. T. Carson, *et al.*, Use of antibacterial consumer products containing quaternary ammonium compounds and drug resistance in the community, *J. Antimicrob. Chemother.*, 2008, **62**(5), 1160–1162.
20 M. S. To, *et al.*, Postadaptational Resistance to Benzalkonium Chloride and Subsequent Physicochemical Modifications of *Listeria monocytogenes*, *Appl. Environ. Microbiol.*, 2002, **68**(11), 5258–5264.
21 J. Aubry, *et al.*, Nanoprecipitation of polymethylmethacrylate by solvent shifting: 1. Boundaries, *Langmuir*, 2009, **25**(4), 1970–1979.
22 K. C. d. Castro, J. M. Costa and M. G. N. Campos, Drug-loaded polymeric nanoparticles: a review, *Int. J. Polym. Mater. Polym. Biomater.*, 2022, **71**(1), 1–13.
23 G. You, *et al.*, Preparation, optimization, characterization and in vitro release of baicalein-solubilizing glycyrrhizic acid nano-micelles, *Int. J. Pharm.*, 2021, **601**, 120546.
24 S. Das, *et al.*, Formulation design, preparation and physicochemical characterizations of solid lipid nanoparticles containing a hydrophobic drug: effects of process variables, *Colloids Surf., B*, 2011, **88**(1), 483–489.
25 A. C. Silva, *et al.*, Long-term stability, biocompatibility and oral delivery potential of risperidone-loaded solid lipid nanoparticles, *Int. J. Pharm.*, 2012, **436**(1–2), 798–805.
26 L. Wu, J. Zhang and W. Watanabe, Physical and chemical stability of drug nanoparticles, *Adv. Drug Delivery Rev.*, 2011, **63**(6), 456–469.
27 M. G. Hemida, *et al.*, The experimental infection with a field isolate of the infectious bronchitis virus from eastern Saudi Arabia resulted in seroconversion of the challenged birds with no apparent clinical diseases, *VirusDisease*, 2021, **32**(2), 354–360.
28 B. Al Tarcha, J. Kojnok and C. Varró, Isolation and characterization of new infectious bronchitis virus variants in Hungary, *Acta Vet. Hung.*, 1990, **38**(4), 287–298.
29 X. Guo, *et al.*, Rapid determination and chemical change tracking of benzoyl peroxide in wheat flour by multi-step IR macro-fingerprinting., *Spectrochim. Acta, Part A*, 2016, **154**, 123–129.
30 O. P. Garcia, *et al.*, Use of lead (II) sulfide nanoparticles as stabilizer for PMMA exposed to gamma irradiation, *Mater. Res.*, 2015, **18**, 365–372.
31 F. Namouchi, *et al.*, Investigation on electrical properties of thermally aged PMMA by combined use of FTIR and impedance spectroscopies, *J. Alloys Compd.*, 2009, **469**(1–2), 197–202.
32 B. Wang, *et al.*, Corrosion inhibition of mild steel by the hydrolysate of an imidazoline-based inhibitor in CO 2-saturated solution, *RSC Adv.*, 2019, **9**(63), 36546–36557.
33 M. Kozak and L. Domka, Adsorption of the quaternary ammonium salts on montmorillonite, *J. Phys. Chem. Solids*, 2004, **65**(2–3), 441–445.
34 M. G. Spirin, S. B. Brichkin and V. F. Razumov, Studies on absorption spectra of uniform gold nanoparticles prepared in Triton X-100 reverse micelles, *J. Photochem. Photobiol., A*, 2008, **196**(2–3), 174–179.
35 M. Karimi, *et al.*, A facile and sustainable method based on deep eutectic solvents toward synthesis of amorphous calcium phosphate nanoparticles: the effect of using

© 2023 The Author(s). Published by the Royal Society of Chemistry

Open Access Article. Published on 21 March 2023. Downloaded on 2/11/2026 2:45:44 PM.
This article is licensed under a Creative Commons Attribution-NonCommercial 3.0 Unported Licence.

various solvents and precursors on physical characteristics, *J. Non-Cryst. Solids*, 2016, **443**, 59–64.

36 M. A. T. Blaskovich, *et al.*, In vitro Antimicrobial Activity of Acne Drugs Against Skin-Associated Bacteria, *Sci. Rep.*, 2019, **9**(1), 14658.

37 L. Decker, D. Deuel and D. Sedlock, Role of lipids in augmenting the antibacterial activity of benzoyl peroxide against Propionibacterium acnes, *Antimicrob. Agents Chemother.*, 1989, **33**(3), 326–330.

38 J. W. Fluhr and K. Degitz, Antibiotics, azelaic acid and benzoyl peroxide in topical acne therapy, *J. Ger. Soc. Dermatol.*, 2010, **8**, S24–S30.

39 K. Okamoto, *et al.*, In vitro antimicrobial activity of benzoyl peroxide against Propionibacterium acnes assessed by a novel susceptibility testing method, *J. Infect. Chemother.*, 2016, **22**(6), 426–429.

40 A. J. Cunliffe, *et al.*, How Do We Determine the Efficacy of an Antibacterial Surface? A Review of Standardised Antibacterial Material Testing Methods, *Antibiotics*, 2021, **10**(9), 1069.

41 A. Perez-Gavilan, *et al.*, Antibacterial activity testing methods for hydrophobic patterned surfaces, *Sci. Rep.*, 2021, **11**(1), 6675.

© 2023 The Author(s). Published by the Royal Society of Chemistry